Stokes flow inside an evaporating liquid line for any contact angle

A. J. Petsi and V. N. Burganos*

Institute of Chemical Engineering and High Temperature Chemical Processes—Foundation for Research and Technology, Hellas and Department of Chemical Engineering, University of Patras, 26504 Patras, Greece

(Received 20 February 2008; revised manuscript received 11 June 2008; published 26 September 2008)

Evaporation of droplets or liquid films lying on a substrate induces internal viscous flow, which affects the transport of suspended particles and, thus, the final deposit profile in numerous applications. In this work, the problem of Stokes flow inside a two-dimensional droplet, representing the cross section of an evaporating liquid line lying on a flat surface, is considered. The stream function formulation is adopted, leading to the biharmonic equation in bipolar coordinates. A solution in closed form is obtained for *any* contact angle in $(0,\pi)$ and is, thus, valid for both hydrophilic and hydrophobic substrates. The solution can be used with any type of evaporation mechanism, including diffusion, convection, or kinetically controlled modes. Both pinned and depinned contact lines are considered. For the boundary conditions to be compatible at the contact lines, the *Navier* slip boundary condition is applied on the substrate. Numerical results are presented for kinetically and diffusion controlled evaporation. For pinned contact lines, the flow inside the evaporating liquid line is directed towards the edges, thus, promoting the coffee stain phenomenon. In the case of depinned contact lines and contact angle less than $\pi/2$, the flow is directed towards the center of the droplet, whereas, for strongly hydrophobic substrates it is directed outwards.

DOI: 10.1103/PhysRevE.78.036324 PACS number(s): 47.55.D−, 47.11.−j, 68.03.Fg, 81.15.Ef

I. INTRODUCTION

In previous publications the authors presented an analytical solution to the problem of potential flow inside an evaporating film, shaped as a cylindrical segment lying on a flat surface [1,2]. This solution elucidated and quantified the flow details during evaporation as these are dictated by the evaporation flux from the surface and by the mobility of the contact lines. The flow direction from the center towards the film edges is held responsible for the appearance of the so-called coffee-stain phenomenon [3,4], which is known to significantly affect the properties and performance of substrate micropatterns in a variety of modern technology applications, including microelectronics [5,6], LED manufacturing [7–9], microlens fabrication [10–12], biosensors [13], biomolecule probing [14], cell culture carriers [15], determination of trace analytes [16], etc.

The evaporation-induced flow inside liquid films shaped as cylindrical segments and lying on a flat substrate was recently exploited successfully by Sharma *et al.* [17] to deposit anisotropic particles in parallel alignment. Specifically, the analytical solution for the potential flow field inside an evaporating liquid line described in [2] was used to describe qualitatively the accumulation of carbon nanotubes suspended in an evaporating liquid line. Although quite useful in interpreting spreading and deposition of suspended particles during film evaporation, the potential flow field cannot be directly used in particle transport calculations, which would necessitate the incorporation of viscous phenomena in the determination of the flow field.

The main difficulty that arises in the study of viscous flow inside evaporating films stems from the increased order of the flow equation compared to that of the potential flow case in combination with nontrivial compatibility issues at the contact lines. However, given the typically small characteristic sizes of droplets and films, it can be shown that viscous effects are expected to dominate over inertial ones [18] so that the *Stokes* flow equation can be used instead. For infinitely long films shaped as cylindrical segments lying on a flat substrate (also termed two-dimensional droplets in the literature), bipolar coordinates are the most suitable coordinates to use in the mathematical formulation of the problem. Even so, a set of two second-order partial differential equations need to be solved for the two velocity components. In the stream function formulation, the biharmonic equation in bipolar coordinates is to be solved coupled with appropriate boundary conditions.

An additional factor that affects drastically the magnitude and the direction of flow inside an evaporating droplet or film is the mobility of the contact lines. More specifically, it has been observed experimentally [3,4,19–26] that pinning of the contact lines induces flow towards the film edges, which are thus replenished and the initial contact area remains wetted. Suspended particles can thus be transferred towards the film edges, yielding a ringlike deposit (coffee-stain phenomenon). On the contrary, if the contact lines are allowed to recede towards the center of the liquid body [3,19–22,26,27], then an inwards liquid motion is expected, which may give rise to a craterlike deposit. Theoretical studies of the internal flow field in evaporating droplets are also available using the vertically averaged liquid velocity [1,2,4,26,28], lubrication theory for small contact angles [18,24,29], direct numerical solution of the creeping flow equation [18], or analytical solutions in the potential flow limit [1,2,30]. The normal component of the liquid velocity at the interface is, in any case, the result of the sum of the mass transfer velocity and the radial component of the interface velocity, the latter expressing the local interface shift per unit of time due to the evaporation of liquid mass. In general, the liquid velocity is different from zero at the contact lines.

*Corresponding author; vbur@iceht.forth.gr

The knowledge of the liquid velocity at the evaporation surface provides a nonhomogeneous boundary condition there, which is used for the derivation of a nontrivial solution to the flow problem. In the potential flow case, fluid slip on the substrate is a natural consequence of the inviscid character of the flow and the corresponding velocity can be allowed to match the liquid velocity at the contact lines. However, in the viscous flow case, some slip flow boundary condition must be employed to achieve this matching at the contact lines. To this end, the Navier slip condition can be used, which relates the slip velocity to the shear stress on the substrate through a slip coefficient. A potential drawback of such a boundary condition is that it may allow for the development of a nonrealistic slip velocity over the entire substrate surface and not only in the neighborhood of the contact lines. A similar problem arises in the modeling of droplet spreading with or without evaporation, in which case the liquid velocity at the contact lines is not defined beforehand, but can be introduced through a Navier slip condition [31,32].

In the present work, the biharmonic equation is solved in bipolar coordinates to obtain an expression for the stream function during evaporation of a two-dimensional viscous droplet with pinned or depinned contact lines, for any contact angle $(0,\pi)$ and for arbitrary evaporation rate profile along the droplet surface. The issue of incompatibility between the various boundary conditions at the contact lines and the no-slip condition on the solid surface is treated through the employment of the classical Navier slip condition, the role of which can be quantitatively adjusted to the requirements at the boundaries of the droplet. A detailed discussion of this point is presented here along with typical numerical results for kinetically and diffusion controlled evaporation of a droplet with pinned or depinned contact lines.

II. MODEL DEVELOPMENT AND SOLUTION

A. Flow field inside an evaporating liquid line

The problem of flow inside an evaporating liquid line lying on a flat surface can be solved on a single cross section if the length of the liquid line is much greater than its width. This is an assumption that holds in many applications. In this case, the liquid line can be approximated by a cylindrical segment thanks to the action of the surface tension [1,2,18,19,30], which minimizes the free surface per unit of volume. The bipolar coordinate system is suitable to describe the liquid-gas as well as the liquid-substrate interfaces [2]. The bipolar coordinates α,β (see Fig. 1) are related to the Cartesian coordinates x,y through $x+iy=c\tanh((\alpha+i\beta)/2)$ [33], which gives

$$x = c\frac{\sinh\alpha}{\cosh\alpha+\cos\beta}, \tag{1a}$$

$$y = c\frac{\sin\beta}{\cosh\alpha+\cos\beta}, \tag{1b}$$

with $-\infty<\alpha<+\infty$, $-\pi<\beta<\pi$, and $c=\text{const}>0$. The liquid-gas interface is attained for $\beta=\theta_c$ and the liquid-solid interface for $\beta=0$, whereas the contact lines are described by $\alpha\to\pm\infty$ and the constant c is equal to half the wetted area width, R_b.

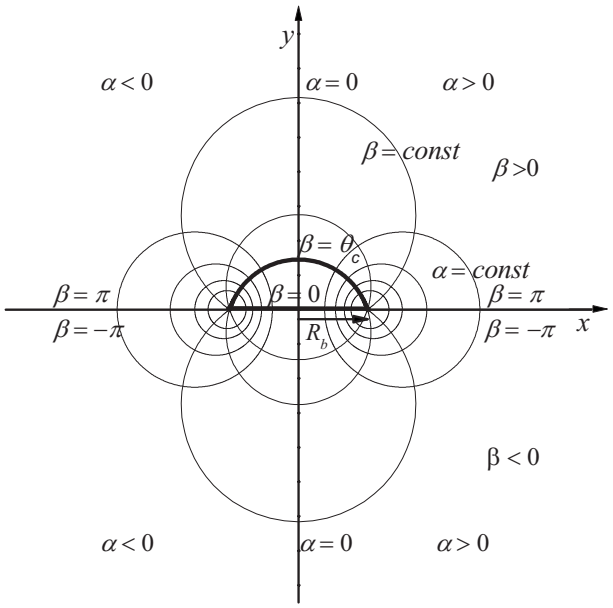

FIG. 1. Bipolar coordinate system and droplet boundaries (bold lines).

The flow inside the liquid body has the characteristics of *Stokes* flow, which is described by the biharmonic equation in the stream function formulation [34]

$$\nabla^4\psi = 0, \tag{2}$$

where ψ is the stream function, and is related to the α- and β-velocity components through the expressions [2]

$$v_\alpha = \frac{\cosh\alpha+\cos\beta}{R_b}\frac{\partial\psi}{\partial\beta}, \tag{3a}$$

$$v_\beta = -\frac{\cosh\alpha+\cos\beta}{R_b}\frac{\partial\psi}{\partial\alpha}. \tag{3b}$$

Following the formulation proposed by Jeffery [35] for elasticity problems in the bipolar coordinate system, the biharmonic equation for the stream function can be written in the form

$$\left(\frac{\partial^4}{\partial\alpha^4}+2\frac{\partial^4}{\partial\alpha^2\partial\beta^2}+\frac{\partial^4}{\partial\beta^4}-2\frac{\partial^2}{\partial\alpha^2}+2\frac{\partial^2}{\partial\beta^2}+1\right)(h\psi)=0, \tag{4}$$

where $h=(\cosh\alpha+\cos\beta)/R_b$.

The boundary conditions that apply in the case of evaporation from the cylindrical surface are:

Finite velocity at the contact lines

$$v_\alpha|_{\alpha\to\pm\infty} = \text{finite}, \tag{5a}$$

$$v_\beta|_{\alpha\to\pm\infty} = \text{finite}, \tag{5b}$$

Zero shear stress at evaporation surface $\tau_{\beta\alpha}|_{\beta=\theta_c}=0$, (5c)

No flow through substrate $v_\beta|_{\beta=0}=0$, (5d)

Normal liquid velocity at evaporation surface $v_\beta|_{\beta=\theta_c}=v_{Ln}$, (5e)

where $v_{Ln}=u_{sn}+J/\rho$, with J the local evaporation flux, u_{sn} the normal component of the surface velocity, and ρ the liquid density.

There is still one more boundary condition that is needed at the liquid-solid interface. The usual no-slip assumption cannot be employed here, since the liquid velocity is generally not equal to zero at the contact lines. A commonly used option is the Navier slip condition [31,32], expressed as $v_x=(\xi/\eta)\tau_{yx}$, where v_x is the liquid velocity component that is parallel to the surface, τ_{yx} is the shear stress, η is the liquid viscosity, and ξ is the slip length. In bipolar coordinates this condition reads as follows:

Navier slip condition $v_\alpha|_{\beta=0}=(\xi/\eta)\ \tau_{\beta\alpha}|_{\beta=0}$. (5f)

Using Eqs. (3a) and (3b), the boundary conditions (5a)–(5f) can be expressed in the stream function formulation as

$$\left(h\frac{\partial\psi}{\partial\beta}\right)\bigg|_{a\to\pm\infty}=\text{finite}, \tag{5a'}$$

$$\left(-h\frac{\partial\psi}{\partial\alpha}\right)\bigg|_{a\to\pm\infty}=\text{finite}, \tag{5b'}$$

$$\left\{h\left[h\left(\frac{\partial^2\psi}{\partial\beta^2}-\frac{\partial^2\psi}{\partial\alpha^2}\right)-\frac{2\sin\beta}{R_b}\frac{\partial\psi}{\partial\beta}-\frac{2\sinh\alpha}{R_b}\frac{\partial\psi}{\partial\alpha}\right]\right\}\bigg|_{\beta=\theta_c}=0, \tag{5c'}$$

$$\left(h\frac{\partial\psi}{\partial\alpha}\right)\bigg|_{\beta=0}=0, \tag{5d'}$$

$$\left(-h\frac{\partial\psi}{\partial\alpha}\right)\bigg|_{\beta=\theta_c}=v_{Ln}, \tag{5e'}$$

$$\left(h\frac{\partial\psi}{\partial\beta}\right)\bigg|_{\beta=0}=\xi\left\{h\left[h\left(\frac{\partial^2\psi}{\partial\beta^2}-\frac{\partial^2\psi}{\partial\alpha^2}\right)-\frac{2\sin\beta}{R_b}\frac{\partial\psi}{\partial\beta}-\frac{2\sinh\alpha}{R_b}\frac{\partial\psi}{\partial\alpha}\right]\right\}\bigg|_{\beta=0}. \tag{5f'}$$

Equation (5e′) allows all the information about the evaporation conditions to be introduced into the problem through v_{Ln}. More specifically, the type of mechanism that controls evaporation (diffusion, phase change, convection) dictates the value of the local evaporation flux, J, whereas the mobility of the contact lines (pinned or depinned) determines the normal component of the surface velocity.

The expressions that provide u_{sn} as a function of the evaporation rate in the cases of pinned and depinned contact lines have been derived in a previous publication by the authors [2] and are given, respectively, by the expressions

$$u_{sn}=-\frac{J_{TOT}}{2\rho R_b}\frac{\sin^3\theta_c}{(\sin\theta_c-\theta_c\cos\theta_c)}\frac{1}{(\cosh\alpha+\cos\theta_c)}, \tag{6a}$$

$$u_{sn}=-\frac{J_{TOT}}{2\rho R_b}\frac{\sin^3\theta_c}{(\theta_c-\sin\theta_c\cos\theta_c)}\frac{\cosh\alpha}{(\cosh\alpha+\cos\theta_c)}, \tag{6b}$$

where J_{TOT} is the total evaporation rate from the droplet surface per unit length, given by

$$J_{TOT}=R_b\int_{-\infty}^{+\infty}\frac{J(\alpha)}{\cosh\alpha+\cos\theta_c}d\alpha. \tag{7}$$

The solution of Eq. (4) subject to the boundary conditions (5a′), (5b′), (5c′), (5d′), (5e′), and (5f′) can be obtained following a method that is conceptually similar to the method used by Jeffery [35], though appropriately adapted to the peculiarities of the problem at hand. More specifically, the general solution of Eq. (4) has the form

$$h\psi=e^{\alpha}F_1(\alpha+i\beta)+e^{-\alpha}F_2(\alpha+i\beta)+e^{\alpha}F_3(\alpha-i\beta)+e^{-\alpha}F_4(\alpha-i\beta).$$

We seek a solution of the type $h\psi=\phi_1(\alpha)\cos\nu\beta$ or $h\psi=\phi_1(\alpha)\sin\nu\beta$, where $\nu=\kappa+i\lambda$ with κ,λ real numbers. Substitution into Eq. (4) gives

$$\left[\frac{d^4}{d\alpha^4}-2(\nu^2+1)\frac{d^2}{d\alpha^2}+(\nu^2-1)^2\right]\phi(\alpha)=0.$$

Making use of the characteristic equation

$$\mu^4-2(\nu^2+1)\mu^2+(\nu^2-1)^2=0,$$

with roots $\mu_1=\nu+1$, $\mu_2=\nu-1$, $\mu_3=-\nu+1$, and $\mu_4=-\nu-1$, we obtain the solution

$$\phi_1(\alpha)=E_1\cosh(\nu+1)\alpha+E_2\sinh(\nu+1)\alpha+E_3\cosh(\nu-1)\alpha+E_4\sinh(\nu-1)\alpha,$$

except for $\nu=0$, which leads to two double roots $\mu_{1,2}=1$ and $\mu_{3,4}=-1$, and for $\nu=1$, which gives one double root $\mu_{1,2}=0$ and two distinct roots $\mu_3=2$ and $\mu_4=-2$. That is,

$$\phi_1(\alpha)=E_1'\cosh\alpha+E_2'\sinh\alpha+E_3'\alpha\cosh\alpha+E_4'\alpha\sinh\alpha$$

for $\nu=0$ and

$$\phi_1(\alpha)=E_1''\cosh 2\alpha+E_2''\sinh 2\alpha+E_3''+E_4''\alpha$$

for $\nu=1$.

We also seek a solution component of the type $h\psi=\phi_2(\beta)\cosh\nu\alpha$ or $h\psi=\phi_2(\beta)\sinh\nu\alpha$ and following the same steps we find that

$$\phi_2(\beta)=D_1\cos(\nu+1)\beta+D_2\sin(\nu+1)\beta+D_3\cos(\nu-1)\beta+D_4\sin(\nu-1)\beta$$

except for $\nu=0$, which gives

$$\phi_2(\beta)=D_1'\cos\beta+D_2'\sin\beta+D_3'\beta\cos\beta+D_4'\beta\sin\beta,$$

and for $\nu=1$, which gives

$$\phi_2(\beta) = D_1'' \cos 2\beta i + D_2'' \sin 2\beta i + D_3'' + D_4''\beta.$$

Since the solution, as the boundary conditions imply, need not be periodical in variable β, the eigenvalues do not have to be positive integer numbers as was the case in the problems solved by Jeffery [35]. Furthermore, the contact lines of the liquid droplet are described by $\alpha \to \pm\infty$, thus necessitating the use of a continuous spectrum for the eigenvalues. Also, the stream function has to be kept finite within the domain of the droplet. Taking the above into account, $\kappa=0$ and $\nu=i\lambda$, and the general solution that applies to this problem is given by

$$h\psi = \int_0^{+\infty} [(A_1 \cosh \alpha + A_2 \sinh \alpha)\cos \lambda\alpha + (A_3 \cosh \alpha + A_4 \sinh \alpha)\sin \lambda\alpha](A_5 \cosh \lambda\beta + A_6 \sinh \lambda\beta)d\lambda + (A_7 \cosh \alpha + A_8 \sinh \alpha)\alpha + \int_0^{+\infty} [(C_1 \cosh \lambda\beta + C_2 \sinh \lambda\beta)\cos \beta + (C_3 \cosh \lambda\beta + C_4 \sinh \lambda\beta)\sin \beta](C_5 \cos \lambda\alpha + C_6 \sin \lambda\alpha)d\lambda + (C_7 \cos \beta + C_8 \sin \beta)\beta. \quad (8)$$

The requirement of finite velocity at the contact lines [Eqs. (5a′) and (5b′)] simplifies Eq. (8) to

$$h\psi = \int_0^{+\infty} [(C_1 \cosh \lambda\beta + C_2 \sinh \lambda\beta)\cos \beta + (C_3 \cosh \lambda\beta + C_4 \sinh \lambda\beta)\sin \beta] \times (C_5 \cos \lambda\alpha + C_6 \sin \lambda\alpha)d\lambda + \beta(C_7 \cos \beta + C_8 \sin \beta). \quad (9)$$

The impermeable substrate boundary condition [Eq. (5d′)] requires constant ψ at $\beta=0$. This constant ψ value can be taken equal to zero, since ψ is always defined within an additive constant. Applying this to Eq. (9) results in $C_1=0$.

The zero shear stress boundary condition [Eq. (5c′)], after some manipulations, can be written as $[\partial^2(h\psi)/\partial\beta^2 - \partial^2(h\psi)/\partial\alpha^2 + h\psi]|_{\beta=\theta_c}=0$. Introducing the expression given in Eq. (9) into this equation, one obtains

$$C_4 = \frac{C_2(\cosh \lambda\theta_c \sin \theta_c - \lambda \sinh \lambda\theta_c \cos \theta_c) - C_3(\sinh \lambda\theta_c \cos \theta_c + \lambda \cosh \lambda\theta_c \sin \theta_c)}{\cosh \lambda\theta_c \cos \theta_c + \lambda \sinh \lambda\theta_c \sin \theta_c}, \quad (10)$$

$$C_7 = C_8 \cos \theta_c / \sin \theta_c. \quad (11)$$

A combination of Eqs. (5d′) and (5f′) leads to

$$\left.\frac{\partial(h\psi)}{\partial\beta}\right|_{\beta=0} = \frac{\xi}{R_b}(\cosh a + 1)\left.\frac{\partial^2(h\psi)}{\partial\beta^2}\right|_{\beta=0}. \quad (12)$$

Introducing expression (9) into Eq. (12) and using Eq. (11), one obtains $C_7=C_8=0$ and

$$\int_0^{+\infty} (\lambda C_2 + C_3)(C_5 \cos \lambda\alpha + C_6 \sin \lambda\alpha)d\lambda = (\xi/R_b)(\cosh \alpha + 1)\int_0^{+\infty} 2\lambda C_4(C_5 \cos \lambda\alpha + C_6 \sin \lambda\alpha)d\lambda. \quad (13)$$

Finally, the introduction of Eq. (9) into Eq. (5e′) gives

$$\int_0^{+\infty} [C_2 \sinh \lambda\theta_c \cos \theta_c + (C_3 \cosh \lambda\theta_c + C_4 \sinh \lambda\theta_c)\sin \theta_c] \times (C_5 \cos \lambda\alpha + C_6 \sin \lambda\alpha)d\lambda = (\cosh \alpha + \cos \theta_c)\int_{-\infty}^{\alpha} \frac{-v_{Ln}}{\cosh u + \cos \theta_c}du. \quad (14)$$

Depending on the controlling evaporation mechanism, typically kinetic or diffusion of the vapor from the surface, and on the motion of the contact lines, an expression for v_{Ln} can be derived and introduced into Eq. (14) for the determination of the unknown coefficients. A common case is that of symmetric evaporation with respect to the y axis. Then, ψ is an odd function in α and is given from

$$\psi = \frac{1}{h}\int_0^{+\infty} (C_2 \sinh \lambda\beta \cos \beta + C_3 \cosh \lambda\beta \sin \beta + C_4 \sinh \lambda\beta \sin \beta)\sin \lambda\alpha d\lambda, \quad (15)$$

where C_6 has been merged into C_2, C_3, C_4 and

$$C_2(\lambda) = \frac{\cosh \lambda\theta_c \cos \theta_c + \lambda \sinh \lambda\theta_c \sin \theta_c}{\sinh \lambda\theta_c \cosh \lambda\theta_c}\Omega(\lambda, \theta_c) - C_3(\lambda)\frac{\sin 2\theta_c}{\sinh 2\lambda\theta_c}, \quad (16)$$

$$C_4(\lambda) = \frac{\cosh \lambda\theta_c \sin \theta_c - \lambda \sinh \lambda\theta_c \cos \theta_c}{\sinh \lambda\theta_c \cosh \lambda\theta_c}\Omega(\lambda, \theta_c) + C_3(\lambda)\frac{\cos^2 \theta_c - \cosh^2 \lambda\theta_c}{\sinh \lambda\theta_c \cosh \lambda\theta_c}, \quad (17)$$

$$\int_0^{+\infty} C_3(\lambda)\left(\frac{\sinh 2\lambda\theta_c - \lambda \sin 2\theta_c}{(\cosh\alpha+1)\sinh 2\lambda\theta_c} + 4\lambda\frac{\xi}{R_b}\frac{\cosh^2\lambda\theta_c - \cos^2\theta_c}{\sinh 2\lambda\theta_c}\right)\sin\lambda\alpha d\lambda$$
$$= \int_0^{+\infty}\lambda\left[2\frac{\xi}{R_b}\left(\frac{\sin\theta_c}{\sinh\lambda\theta_c} - \frac{\lambda\cos\theta_c}{\cosh\lambda\theta_c}\right) - \left(\frac{\lambda\sin\theta_c}{\cosh\lambda\theta_c} + \frac{\cos\theta_c}{\sinh\lambda\theta_c}\right)\frac{1}{(\cosh\alpha+1)}\right]\Omega(\lambda,\theta_c)\sin\lambda\alpha d\lambda, \quad (18)$$

$$\Omega(\lambda,\theta_c) = -\frac{2}{\pi}\int_0^{+\infty}(\cosh\alpha+\cos\theta_c) \times\left(\int_{-\infty}^{\alpha}\frac{v_{Ln}}{\cosh\alpha'+\cos\theta_c}d\alpha'\right)\sin\lambda\alpha d\alpha. \quad (19)$$

At this point it is worth mentioning that the same solution would be obtained if a different approach was used, namely, the one that takes advantage of the fact that any biharmonic function in (x,y) coordinates can be reproduced using two arbitrary independent harmonic functions f_i, g_i. For instance, it can be expressed as xf_1+g_1, yf_2+g_2, $(x^2+y^2)f_3+g_3$, or as an appropriate combination of these functions [36]. The solution can then be constructed in a step-by-step fashion, as dictated progressively by the boundary conditions of the problem [37,38]. In this way, an expression identical to Eq. (15) can be eventually derived, which is compatible with the boundary conditions (5a′), (5b′), and (5d′), and with the symmetric evaporation rate with respect to the y axis. Then, Eqs. (5c′), (5e′), and (5f′) can be used for the determination of the unknown coefficients C_2, C_3, C_4.

B. Case study: Kinetically controlled evaporation

Assuming slow phase change compared to vapor diffusion, evaporation becomes kinetically controlled and, thus, the evaporation flux remains constant along the surface of the droplet,

$$J(\alpha) = \text{const} = J_0. \quad (20)$$

This evaporation mechanism is dominant in several practical applications, including, for instance, evaporation under vacuum, low temperature evaporation, evaporation of nonvolatile solvents, etc. In this case, using Eqs. (7) and (6a) or (6b), v_{Ln} is given by

$$v_{Ln} = \frac{J_0}{\rho}\left(1 - \frac{\theta_c\sin^2\theta_c}{(\sin\theta_c - \theta_c\cos\theta_c)}\frac{1}{(\cosh\alpha+\cos\theta_c)}\right), \quad (21a)$$

or

$$v_{Ln} = \frac{J_0}{\rho}\left(1 - \frac{\theta_c\sin^2\theta_c}{(\theta_c - \sin\theta_c\cos\theta_c)}\frac{\cosh\alpha}{(\cosh\alpha+\cos\theta_c)}\right) \quad (21b)$$

in bipolar coordinates, for pinned and depinned contact lines, respectively.

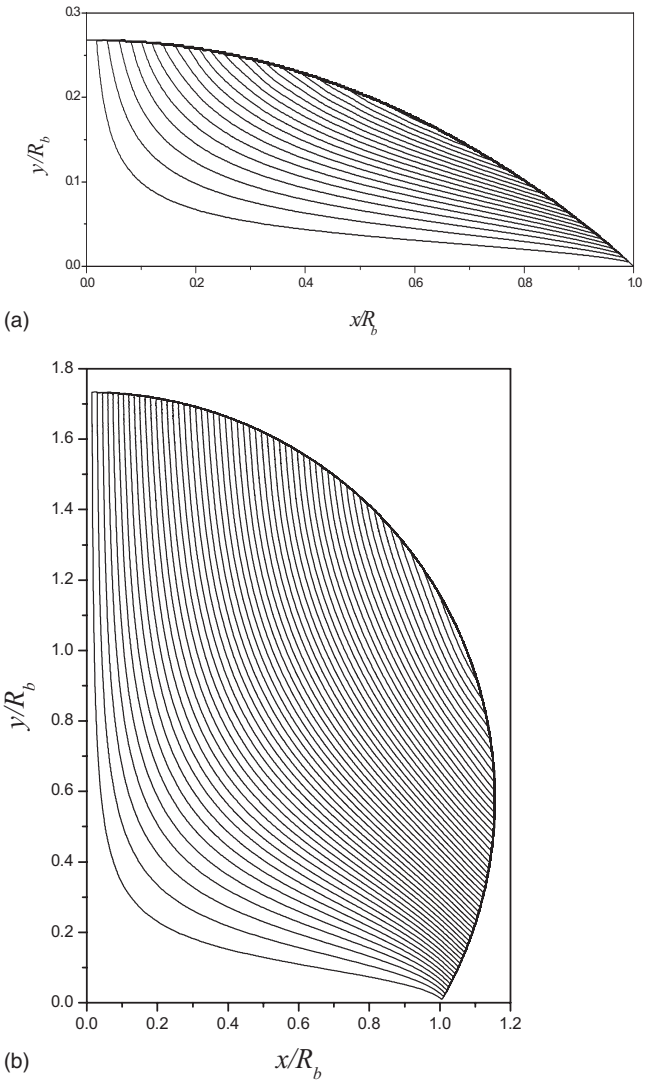

FIG. 2. Streamlines ($\delta\psi$=0.01) inside a kinetically controlled evaporating droplet with pinned contact lines and contact angle: (a) $\theta_c=\pi/6$ and (b) $\theta_c=2\pi/3$.

Substituting Eqs. (21a) and (21b) into Eq. (19), the coefficients C_2, C_3, C_4 can be calculated using Eqs. (16)–(18). Evaluation of the coefficient $C_3(\lambda)$ from Eq. (18) can be done numerically at discrete λ values. Then, the stream function and the local velocity can be obtained from Eqs. (15) and (3), respectively.

III. RESULTS AND DISCUSSION

In this section, numerical results for the viscous flow field that develops in the interior of an evaporating liquid line lying on a flat impermeable substrate are presented. Kinetically controlled evaporation is considered first. In Figs. 2(a) and 2(b) the streamlines for the case of pinned contact lines are plotted for $\theta_c=\pi/6$ and $\theta_c=2\pi/3$, respectively. The same, constant stream function step was used in these two figures for the sake of comparison of the two flow fields. It was found that flow is directed from the center to the edges in the case of pinned contact lines for any value of the con-

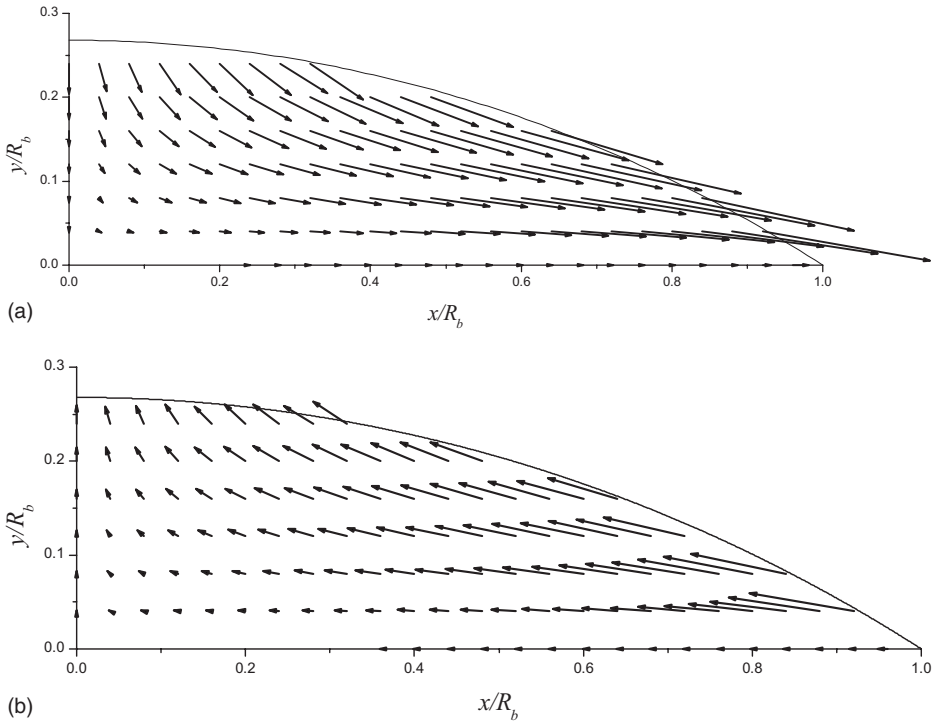

FIG. 3. Vector representation of the internal flow field in a kinetically controlled evaporating droplet with contact angle $\theta_c = \pi/6$, dimensionless slip coefficient $\bar{\xi}=10^{-3}$, and (a) pinned contact lines and (b) depinned contact lines.

tact angle $(0,\pi)$. If the contact lines are depinned during evaporation, then for any value of the contact angle $(0,\pi/2)$, the liquid flow is directed towards the center of the liquid line. However, for contact angles greater than $\pi/2$ and depinned contact lines the flow field is directed towards the contact lines, whereas for contact angle $\theta_c=\pi/2$ no flow develops inside the droplet since v_{Ln} becomes zero. The vector representation of the flow field for $\theta_c=\pi/6$ is shown in Figs. 3(a) and 3(b) for pinned and depinned contact lines, respectively. It is interesting to note that for the same contact angle and the same evaporation rate, the local velocity magnitude is larger in the case of pinned contact lines than that in the case of depinned contact lines.

All the results presented in Figs. 2 and 3 were obtained for $\bar{\xi}=\xi/R_b=10^{-3}$. In Fig. 4 the fluid velocity on the substrate surface is plotted against the distance from the center of the droplet for different values of ξ/R_b. As ξ/R_b decreases to very small values, the slip velocity tends to zero over the entire substrate except for a very narrow zone close to the contact lines, where it takes up the required magnitude to match the velocity that is imposed by the boundary condition there. Hence, the solution may also be, practically, compatible with the requirement of no slip at the wall in the bulk of the wetted area, allowing only some finite slip near the contact lines. Obviously, if the evaporation velocity is taken to be zero at the contact lines [29] and the interface velocity is also zero there ($u_{sn}=0$, as in the case of pinned contact lines), the liquid velocity is zero at the contact lines and the no-slip condition can be applied. In the case of depinned contact lines, this is true only if the evaporation velocity is equal in magnitude and opposite in sign to the velocity of the contact lines as they recede towards the center of the droplet, following the equation

$$v_{Ln} = u_{sn} + J(\alpha \to \infty, \beta = \theta_c)/\rho. \tag{22}$$

In any other case, the liquid velocity at the contact lines is different from zero and some slip velocity must be allowed. For the sake of completeness, the analytical expression for the coefficients C_2, C_3, and C_4 for $\xi=0$ (no slip) are given below.

$$C_2(\lambda) = \frac{\cosh \lambda\theta_c \cos\theta_c + \lambda \sinh \lambda\theta_c \sin\theta_c}{\sinh \lambda\theta_c \cosh \lambda\theta_c - \lambda \sin\theta_c \cos\theta_c}\Omega(\lambda,\theta_c), \tag{23a}$$

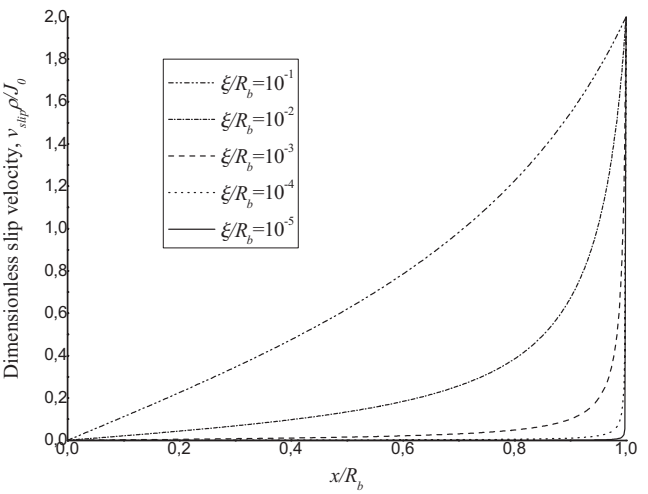

FIG. 4. Dimensionless slip velocity vs dimensionless distance from the center of the droplet for pinned contact lines, $\theta_c=\pi/6$ and for various values of the slip coefficient.

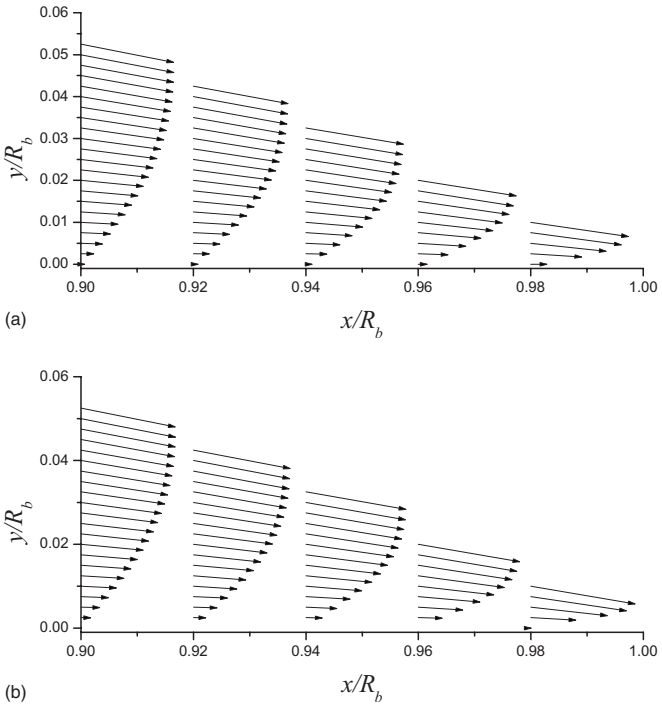

FIG. 5. Vector representation of the internal flow field near the contact lines in a kinetically controlled evaporating droplet with pinned contact lines, contact angle $\theta_c=\pi/6$, and dimensionless slip coefficient (a) $\bar{\xi}=10^{-3}$ and (b) $\bar{\xi}=10^{-5}$.

$$C_3(\lambda) = -\lambda \frac{\cosh \lambda\theta_c \cos\theta_c + \lambda \sinh \lambda\theta_c \sin\theta_c}{\sinh \lambda\theta_c \cosh \lambda\theta_c - \lambda \sin\theta_c \cos\theta_c} \Omega(\lambda, \theta_c), \tag{23b}$$

$$C_4(\lambda) = \frac{(1+\lambda^2)\cosh \lambda\theta_c \sin\theta_c}{\sinh \lambda\theta_c \cosh \lambda\theta_c - \lambda \sin\theta_c \cos\theta_c} \Omega(\lambda, \theta_c), \tag{23c}$$

where $\Omega(\lambda, \theta_c)$ is given from Eq. (19).

It is noteworthy that the internal flow field is not sensitive to the slip coefficient for ξ/R_b values less than 10^{-3}. Figure 5 shows a vector representation of the flow field near the contact lines, assuming them pinned, for $\theta_c=\pi/6$ and for two values of the slip coefficient, namely, $\xi/R_b=10^{-3}$ [Fig. 5(a)] and $\xi/R_b=10^{-5}$ [Fig. 5(b)]. A very weak effect of the slip coefficient on the flow field near the contact lines is discerned, which, however, leaves the flow field throughout the rest of the droplet region, practically unaffected. Needless to say, the use of a much larger slip coefficient would certainly affect the local flow field more significantly; however, it would also lead to unrealistically large slip velocity far from the contact lines.

In the case of pinned contact lines, the flow field would direct colloidal particles towards the contact lines, thus promoting their accumulation and deposition there. This has been repeatedly observed in experiments involving colloidal suspensions [4,19,21–25]. On the contrary, if the contact lines are depinned and the contact angle is less than $\pi/2$, the flow is directed towards the center of the liquid line, thus promoting deposition away from the contact lines. This behavior has also been observed experimentally [21,22,25]. If the contact lines are depinned and the contact angle is greater than $\pi/2$, the flow is directed towards the contact lines just like in the pinned case. However, as the contact line recedes it is reasonable to expect that the suspended particles will be progressively deposited over the entire area that was initially wetted by the droplet.

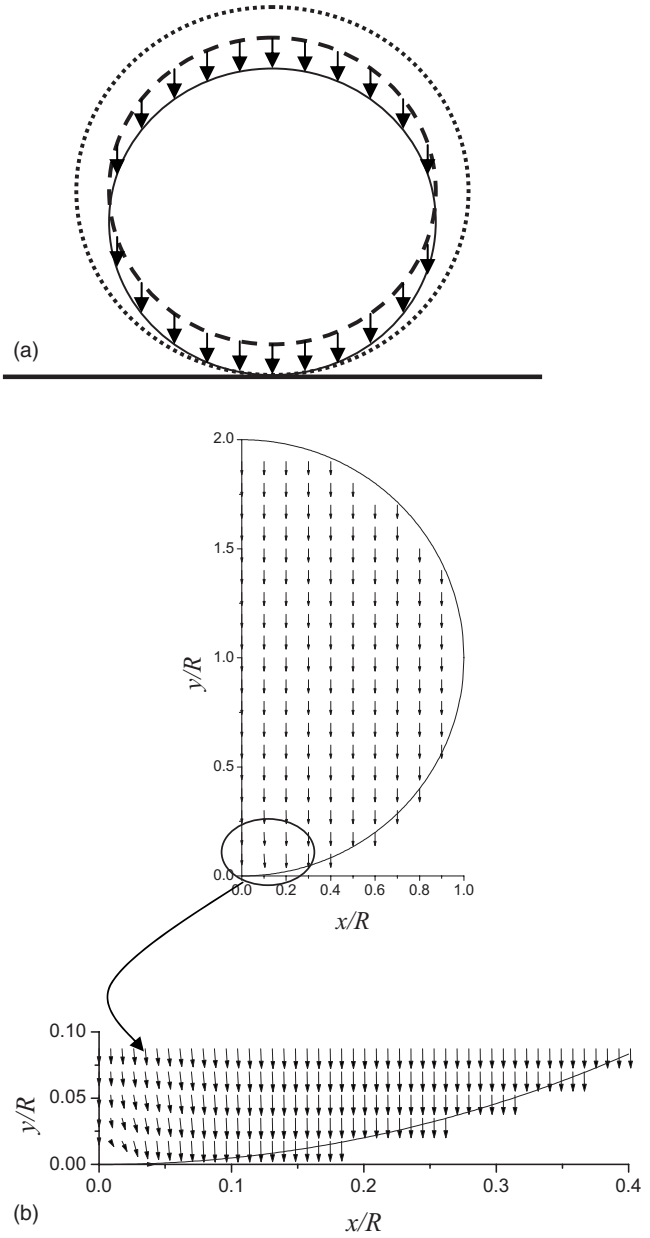

FIG. 6. (a) Schematic representation of liquid boundaries during evaporation of a droplet with $\theta_c=\pi$. The dotted line represents the boundary prior to evaporation, the dashed line represents the hypothetic boundary in the absence of any contact with the substrate, and the solid line represents the boundary after the evaporation step. Vectors show the flow direction. (b) Vector representation of the internal flow field in a kinetically controlled evaporating droplet with constant contact angle $\theta_c=179\pi/180$. Inset: Detail of the flow field in the vicinity of the contact area.

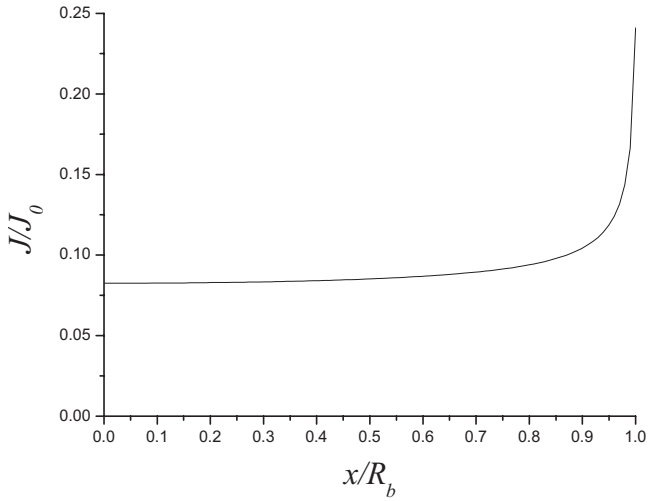

FIG. 7. Profile of evaporation flux corresponding to diffusion-controlled evaporation for pinned contact lines and $\theta_c=\pi/3$.

It would be interesting to see what happens in the extreme case of contact angle equal to π. In this case the droplet of radius R touches only tangentially the substrate and if it is assumed that it keeps doing so during evaporation, then it can be shown that a uniform flow field develops in a direction normal to the substrate [Fig. 6(a)]. Specifically, since the wetted area is diminished, uniform evaporation from the surface would result in uniform shrinking of the droplet (dashed line). However, the need to retain a single contact point with the substrate implies a vertical shift to the final position (solid line), corresponding to the uniform, vertical velocity that was mentioned above. The solution for the internal flow field inside an evaporating droplet that was derived in bipolar coordinates cannot be directly applied to this particular case, since the two poles of the bipolar system coincide for $\theta_c=\pi$. However, as $\theta_c\rightarrow\pi$ the flow field that results from the solution in the bipolar system reproduces closely the uniform flow field, as shown in Fig. 6(b) (the value $\theta_c=179\pi/180$ was used in these calculations). Some small deviation of this flow field from uniform velocity field is seen in the inset of Fig. 6(b) and is due to the presence of a finite wetted area ($R_b/R=\sin\theta_c\simeq 0.017$ in this illustration).

It is also interesting to see how a different profile of evaporation flux along the liquid surface would affect the flow field. The expression $J(x)=J_0^D[b_1/\sqrt{b_2-(x/R_b)^2}+b_3]$ reproduces with good approximation the diffusion flux for $\theta_c=\pi/3$ as presented in [39], where $J_0^D=2Dc_s(1-\theta_c/\pi)/R_b$, D is the vapor diffusion coefficient, c_s is the vapor concentration at the surface of the droplet, x is the distance from the center of the droplet and b_1, b_2, b_3 are numerical constants with values that depend on the contact angle and the outer boundary at which the vapor concentration diminishes. In the present illustration the values $b_1=0.0176$, $b_2=1.01$, $b_3=0.065$ were used, which correspond to the flux profile of Fig. 7. Figure 8 compares the flow field that is obtained in this case with the one that corresponds to uniform evaporation flux (case of kinetically controlled evaporation). To make the comparison quantitative, the ratio $J_0^D/J_0=10.67$ was used in the calculations, so that the total evaporation rate from the liquid surface is the same in both cases. It is seen that the effect of the nonuniformity of the evaporation flux on the flow field is rather limited (faster flow near the contact lines), owing obviously to the fact that the evaporation flux profile in the diffusion controlled case remains practically uniform over a large part of the surface and it is only at the vicinity of the contact lines where some interesting change is noted.

IV. CONCLUDING REMARKS

The problem of Stokes flow that is generated by evaporation inside a liquid line, shaped as a cylindrical segment lying on a flat surface, was considered and a solution for the stream function in closed form was derived. The solution is valid for any mechanism of evaporation, for both pinned and depinned contact lines, provided that the profile of the local evaporation flux on the droplet surface is known.

Numerical results in the case of slow phase change compared to vapor diffusion, implying kinetically controlled evaporation, were presented. Pinned contact lines force liquid to flow towards the edges of the cylindrical segment in order to replenish the area that is evacuated there, thus promoting the well known coffee-stain phenomenon. In the case of depinned contact lines, if the contact angle is smaller than $\pi/2$, flow is directed towards the center of the droplet in

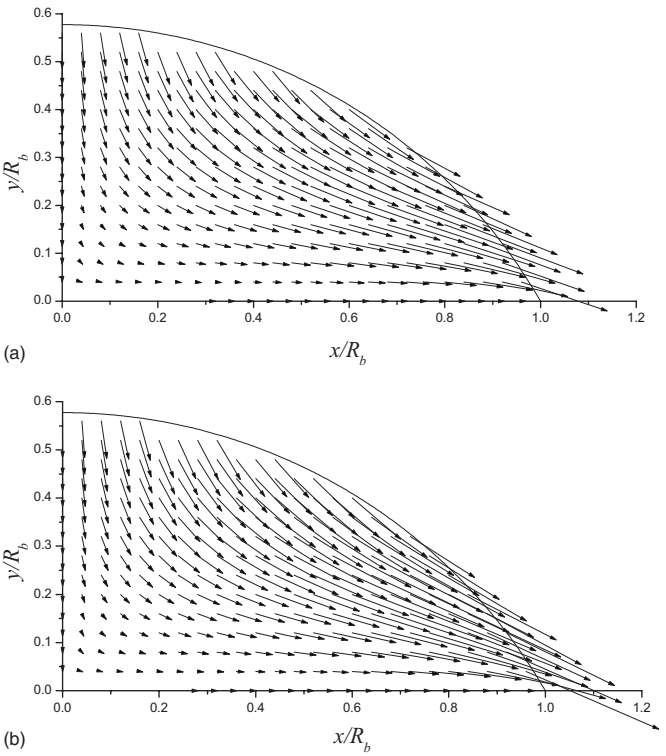

FIG. 8. Vector representation of the internal flow field inside an evaporating droplet with pinned contact lines, contact angle $\theta_c=\pi/3$, and dimensionless slip coefficient $\bar{\xi}=10^{-3}$. Comparison between (a) kinetically and (b) diffusion-controlled cases.

order to ensure constant contact angle and satisfy the requirement of cylindrical shape. For a contact angle larger than $\pi/2$ the flow field has the same direction as that in the pinned contact lines mode. The viscous flow field is qualitative similar to the potential flow field that was calculated in a previous publication [2]; however, the viscous character of the actual flow affects quantitatively the flow field details, which in turn are expected to affect the motion of suspended particles during evaporation. The quantitative study of this process is the subject of ongoing work by the authors. In fact, given the availability of an analytical solution for the viscous flow field at any contact angle, deposition calculations can be extended over the entire duration of the evaporation process.

It has to be mentioned that in order for the boundary conditions to be compatible at the contact lines, combining the boundary conditions (5c′) and (5e′), and the requirement that the fluid velocity should have a unique single value at the contact lines, after algebraic manipulations, the following relation is obtained:

$$\cos 2\theta_c \left[(\cosh\alpha + 1)^2 \frac{\partial^2 \psi}{\partial \beta^2} \right] \Bigg|_{\substack{\beta=0 \\ \alpha \to \pm\infty}} + 2 \sin 2\theta_c \left\{ (\cosh\alpha + 1) \left[(\cosh\alpha + 1) \frac{\partial^2 \psi}{\partial \alpha \partial \beta} + \sinh\alpha \frac{\partial \psi}{\partial \beta} \right] \right\} \Bigg|_{\substack{\beta=0 \\ \alpha \to \pm\infty}} = 0.$$

For $\theta_c = \pi/2$, one obtains $(\cosh\alpha+1)^2(\partial^2\psi/\partial\beta^2)|_{\substack{\beta=0 \\ \alpha\to\pm\infty}} = 0$, which, combined with the Navier slip condition, Eq. (5f′), discloses an incompatibility with the boundary condition for the normal component of the liquid velocity at the surface, Eq. (5e′). To circumvent this problem, a different approach is already in progress by the authors to treat the particular case of $\theta_c = \pi/2$ making use of the polar coordinate system. Nevertheless, in practice, the flow field in this case can be obtained with the help of the solution in bipolar coordinates derived in the present work, using a contact angle value arbitrarily close to $\pi/2$.

[1] A. J. Petsi and V. N. Burganos, Phys. Rev. E **72**, 047301 (2005).
[2] A. J. Petsi and V. N. Burganos, Phys. Rev. E **73**, 041201 (2006).
[3] R. D. Deegan, O. Bakajin, T. F. Dupont, G. Huber, S. R. Nagel, and T. A. Witten, Nature (London) **389**, 827 (1997).
[4] R. D. Deegan, O. Bakajin, T. F. Dupont, G. Huber, S. R. Nagel, and T. A. Witten, Phys. Rev. E **62**, 756 (2000).
[5] K. Cheng, M.-H. Yang, W. W. W. Chiu, C.-Y. Huang, J. Chang, T.-F. Ying, and Y. Yang, Macromol. Rapid Commun. **26**, 247 (2005).
[6] T. Kawase, T. Shimoda, C. Newsome, H. Sirringhaus, and R. H. Friend, Thin Solid Films **438-439**, 279 (2003).
[7] T. Shimoda, K. Morii, S. Seki, and H. Kiguchi, MRS Bull. **28**, 821 (2003).
[8] Y. Xia and R. H. Friend, Appl. Phys. Lett. **88**, 163508 (2006).
[9] Y. Xia and R. H. Friend, Appl. Phys. Lett. **90**, 253513 (2007).
[10] E. Bonaccurso, H.-J. Butt, B. Hankeln, B. Niesenhaus, and K. Graf, Appl. Phys. Lett. **86**, 124101 (2005).
[11] G. Li, N. Höhn, and K. Graf, Appl. Phys. Lett. **89**, 241920 (2006).
[12] R. Pericet-Camara, A. Best, S. K. Nett, J. S. Gutmann, and E. Bonaccurso, Opt. Express **15**, 9877 (2007).
[13] A. P. Sommer, E. Gheorghiu, M. Cehreli, A. R. Mester, and H. T. Whelan, Cryst. Growth Des. **6**, 492 (2006).
[14] V. Kopecký, Jr. and V. Baumruk, Vib. Spectrosc. **42**, 184 (2006).
[15] M. Herklotz, M. Melamed, C. Trautmann, M. Nitschke, T. Pompe, F. U. Gast, F. Howitz, and C. Werner, Microfluid. Nanofluid. **3**, 629 (2007).
[16] Y. Liu, Y. F. Li, and C. Z. Huang, J. Anal. Chem. **61**, 647 (2006).
[17] R. Sharma, C. Y. Lee, J. H. Choi, K. Chen, and M. S. Strano, Nano Lett. **7**, 2693 (2007).
[18] H. Hu and R. G. Larson, Langmuir **21**, 3963 (2005).
[19] W. Jia and H. Qiu, Int. J. Heat Mass Transfer **45**, 4141 (2002).
[20] C. Bourgès-Monnier and M. E. R. Shanahan, Langmuir **11**, 2820 (1995).
[21] K. Uno, K. Hayashi, T. Hayashi, K. Ito, and H. Kitano, Colloid Polym. Sci. **276**, 810 (1998).
[22] B.-J. de Gans and U. S. Schubert, Langmuir **20**, 7789 (2004).
[23] E. Bormashenko, Y. Bormashenko, R. Pogreb, O. Stanevsky, G. Whyman, T. Stein, M. H. Itzhaq, and Z. Barkay, Colloids Surf., A **290**, 273 (2006).
[24] M. Chopra, L. Li, H. Hu, M. A. Burns, and R. G. Larson, J. Rheol. **47**, 1111 (2003).
[25] H.-Y. Ko, J. Park, H. Shin, and J. Moon, Chem. Mater. **16**, 4212 (2004).
[26] J.-H. Kim, S. I. Ahn, J. H. Kim, and W.-C. Zin, Langmuir **23**, 6163 (2007).
[27] M. Cachile, O. Bénichou, and A. M. Cazabat, Langmuir **18**, 7985 (2002).
[28] Y. O. Popov, Phys. Rev. E **71**, 036313 (2005).
[29] B. J. Fischer, Langmuir **18**, 60 (2002).
[30] Y. Y. Tarasevich, Phys. Rev. E **71**, 027301 (2005).
[31] D. M. Anderson and S. H. Davis, Phys. Fluids **7**, 248 (1995).
[32] L. M. Hocking, Phys. Fluids **7**, 2950 (1995).
[33] N. N. Lebedev, I. P. Scalskaya, and Y. S. Uflyand, *Worked Problems in Applied Mathematics* (Dover Publications, Inc., New York, 1965); P. Moon and D. E. Spencer, *Field Theory Handbook* (Springer-Verlag, Berlin, 1961).
[34] L. G. Leal, *Laminar Flow and Convective Transport Prosseses: Scaling Principles and Asymptotic Analysis* (Butterworth-Heinemann, Boston, 1992).
[35] G. B. Jeffery, Philos. Trans. R. Soc. London, Ser. A **221**, 265 (1921).
[36] V. V. Meleshco, Appl. Mech. Rev. **56**, 33 (2003).
[37] A. M. J. Davis and M. E. O'Neill, Q. J. Mech. Appl. Math. **30**, 355 (1977).
[38] S. Wakiya, J. Phys. Soc. Jpn. **39**, 1113 (1975).
[39] A. L. Yarin, J. B. Szczech, C. M. Megaridis, J. Zhang, and D. R. Gamota, J. Colloid Interface Sci. **294**, 343 (2006).